



University of
Salford
MANCHESTER

Strain mapping

Webster, PJ

Title	Strain mapping
Authors	Webster, PJ
Type	Book Section
URL	This version is available at: http://usir.salford.ac.uk/id/eprint/396/
Published Date	2003

USIR is a digital collection of the research output of the University of Salford. Where copyright permits, full text material held in the repository is made freely available online and can be read, downloaded and copied for non-commercial private study or research purposes. Please check the manuscript for any further copyright restrictions.

For more information, including our policy and submission procedure, please contact the Repository Team at: usir@salford.ac.uk.

12 Strain mapping

P. J. Webster

12.1 Introduction

Neutron strain scanning techniques have been developing since the early 1980s U-3J and synchrotron X-ray techniques rapidly since the 1990s [4, 5]. The first neutron measurements used single detector instruments at medium flux reactor sources, 'gauge volumes' that were relatively large and coarsely defined, manual positioning of samples and computer-aided but labour-intensive Interactive Gaussian peak fitting routines. Statistical data quality was often high but spatial resolution, data collection rates and data processing speeds were all relatively low. Even in comparatively simple experiments, for example, scans through thin sections of ferritic steel test samples with moderate residual strain gradients, only a handful of measurements could be made and processed in a day. Consequently most neutron strain investigations were restricted to linear scans at a dozen or so points, usually in three orthogonal directions so that stresses could be derived. Area mapping, which typically might require orthogonal measurements at a hundred or more points was not then generally a practical proposition due to time and resource cost considerations.

With the introduction of high flux neutron sources, multidetectors, automated sample positioning, optimisation of data acquisition, fast and cheap computers, fully computerised peak fitting and commercial surface fitting software, the situation has changed dramatically. The data for an adequately defined neutron diffraction peak might now be collected in a few minutes, or even less, and be processed near on-line, so that multipoint neutron area strain scanning is now practicable [6,7].

Synchrotrons produce near-parallel X-ray beams with extremely high photon fluxes, typically billions of times the equivalent neutron flux of even the most powerful nuclear reactors. On the other hand X-ray attenuation lengths, at similar wavelengths to those used with neutron strain scanning (1 ~ 1.5 Å), tend to be several orders of magnitude smaller than the corresponding neutron attenuation lengths. Consequently, at these wavelengths the attenuation of X-ray beams is generally much higher than for neutron beams, especially through thick samples. However, for harder more penetrating X-rays (Å ~ 0.3 Å), attenuation lengths can be similar (~mm), for light element materials, to those for neutrons. Scattering parameters and attenuation lengths for neutrons and for X-rays of typically used wavelengths are shown for elements that comprise the majority component of common engineering alloys in Table 12.1. In favourable circumstances, such as when measuring through relatively thin samples made of lower attenuating light element materials, synchrotron X-ray count rates, even with single detector instruments, can be orders of magnitude greater than is typical for neutron count rates. Furthermore, synchrotron technology is advancing rapidly, producing higher fluxes at even higher energies. At wiggler and undulator locations synchrotron X-ray

Table 12.1 Neutron and X-ray scattering parameters for four elements which comprise the majority component of many common engineering alloys

Element:	Al	Cu	Fe	Ni
Atomic number	13	29	26	28
Neutron scattering length (fm)	3.45	-3.44	9.45	10.3
Neutron attenuation length (mm)	100	20	8.3	5.6
1.5 Å X-ray attn. length (mm)	0.083	0.012	0.004	0.003
0.3 Å X-ray attn. length (mm)	6.71	1.06	0.38	0.27
0.15 Å X-ray attn. length (mm)	52.6	3.47	3.03	2.19

Note

The scattering length L is the thickness of material required to attenuate a beam by the factor e^{-1} . It is the reciprocal of the linear attenuation coefficient μ , so the intensity I after a thickness x is $I = I_0 e^{-\mu x} = I_0 e^{-x/L}$.

fluxes are particularly high. When used with area detectors, data from several reflections, at all orientations within a nearly flat cone, may be simultaneously recorded in seconds or less. Consequently, although synchrotron strain scanning is a relatively new technique, synchrotron area strain mapping is developing rapidly. As developments proceed it is probable that volume strain mapping will also become routine.

The aim of this chapter is to outline the methods used in neutron and synchrotron strain mapping and to illustrate by examples the potentials of the two techniques,

12.2 Optimisation and efficient strain scanning

12.2.1 Resolution cost

Neutron and synchrotron strain scanning both require large, high capital cost, central facilities that are often used on a timeshare basis. Generally both the demand for and the cost of beam-time are relatively high. As beam-time is usually a large fraction of the total resource cost, it is essential to make efficient use of it. Time for academic investigations is usually restricted and competitively allocated, and commercial use is cost sensitive. The time required for an experiment, using an incrementally stepped detector, is proportional to the scan range and inversely proportional to the sample volume. In a routine synchrotron neutron diffraction experiment to determine the structure of a powdered material, for example, the incident and detected beam cross-sections might be about 40 mm high and 10 mm wide giving a scattering volume about 4000 mm³. The detector scan range to obtain a full diffraction pattern might be $\sim 100^\circ$. Strain scanning is particularly profitable in its use of neutrons or X-ray photons. In neutron strain scanning the beam cross-section might be reduced to 2 x 2 mm giving, with a 2 mm wide detector slice, a 'gauge volume' of 8 mm³. The scan range required to define a single peak might be 2° . For the powder diffraction experiment the time required would be proportional to $100/4000$ and for strain scanning $2/8$. Hence, it would typically be necessary to count about 10 times longer to collect the data for one peak profile when measuring strain than is needed for a complete powder diffraction experiment, if similar peak counts are required. Additionally, strain scanning requires multipoint measurements, usually in three orientations, and precise sample positioning. Consequently, unless appropriate measures are taken, the time required for strain scanning could be hundreds of

thousands of Lines longer than for routine powder diffraction experiments, which would be impractical.

12.2.1.1 MultiDetectors

It is now common, when neutron strain scanning, to use multisectors or position sensitive detectors subtending a few degrees so that data from across the profile of a selected peak can be collected at the same time rather than sequentially. Using a multidetector might typically provide a gain in speed by a factor of 10x, but can introduce potentially severe instrumental aberrations at surfaces and interfaces. Multidetectors can also, of course, provide similar gains for routine powder diffraction experiments so that, although there is a real gain in efficiency when strain scanning, there may be little improvement in competitive advantage relative to powder diffraction.

12.2.1.2 Setting-up and positioning time

initial setting-up of the scanner and precise positioning of the gauge relative to the 'reference point' can be time-consuming, as can be the initial positioning of the sample. Subsequently the time taken to automatically move the sample when scanning can also be a significant proportion of the total time required, particularly when counting times are short.

Well-designed dedicated strain scanners, setting-up times should be short and the gauge volume should, after initial calibration, be automatically adjustable and be precisely positioned at a reference point on the scanner axis. Initial sample positioning is facilitated if the XYZ sample translation and rotation equipment has a precise positioning, orienting and fixing system, preferably conforming to a common standard. This should enable a sample to be positioned off-line on a standard matching mount to within 0.1 mm and aligned to better than 0.1° , before incurring beam-time costs. Efficient rapid mounting, and final position refinement as necessary, is then possible at minimum beam-time cost on-line on the scanner.

The time taken to move the sample when scanning depends upon the inertia of the system and the mechanics, electronics and control software. Time can be saved if the system is designed so that movements can be rapidly, smoothly and precisely executed without significant delay due to over- or under-shooting. Generally, it should be possible to reset the system, when scanning in small steps, in not more than a few seconds. The reduction of dead-time is likely to become an increasingly important factor, especially for synchrotron experiments, as data collection rates increase.

12.2.1.3 Gauge size

Gauge volume sizes should be as large as is practicable considering the instrumental optics, the spatial resolution that is required and attenuation lengths. Minimum gauge sizes tend to be limited by beam divergence when neutron strain scanning, and by grain size considerations when using near-parallel synchrotron X-radiation.

12.2.2 Peak profile determination

The peak profile parameters generally required are: peak centre to determine macro strain, peak width which is a measure of plastic deformation and microstrain, and peak height and intensity which are indicators of texture and grain size.

The longer the count time the better the statistical data quality, which is a function of $1/\sqrt{N}$, where N is the neutron or X-ray photon count, but the fewer the number of points that can be sampled in a given time. The number of data points is linearly related to the time available, but the data quality improves as the square of the time. To optimise the utilisation of counting time, it is necessary to compromise between data quality and quantity. Usually, once the data are adequate to enable a specified statistical uncertainty in strain to be attained, counting time is more efficiently utilised if additional points, rather than statistically improved points, are obtained, especially in area and volume strain mapping. Optimisation of data collection and processing is discussed in Ref. [8]. Particular factors to be considered are the following.

Peak angular range - This should be large enough to define the peak profile and background but not much more. A practical range for a centred Gaussian peak is $3W$ or 3σ , where W is the full width at half maximum (FWHM) and σ is the standard deviation ($W = 2.35\sigma$ for a Gaussian; so that $3\sigma \sim 1.3W$).

Number of points/bins in a peak profile - It is generally found that 20-30 or so points is near-optimum to visually define a peak with a near-Gaussian single peak profile and flat background.

Counts in the peak - Assuming that the background is low, the statistical uncertainty U_c in a near-Gaussian peak position is:

$$U_c = 2.3W/\sqrt{C_T} \quad (1)$$

where C_T is the total neutron or photon count in the peak. The corresponding uncertainty in strain U_ϵ is:

$$U_\epsilon \sim (1/3)W \cot \theta / \sqrt{C_T} \quad (2)$$

where θ is the Bragg angle of the peak and the peak width W is in radians.

Hence a total count of $C_T \sim 4500$ (equivalent to a 21-step, $W/17$ increment, $3W$ range, peak of height $6D$ with a low background) will result in an uncertainty $U_c \sim 1\% W$. For neutron strain scanning at a detector angle $2\theta = 90^\circ$ and typical peak width 0.5° , the corresponding uncertainty in strain is $U_\epsilon \sim 40 \times 10^{-6}$. For the same conditions when synchrotron strain scanning at a typical detector angle $2\theta = 1W$ and peak width 0.04° the uncertainty in strain is approximately the same. If a strain uncertainty $U_\epsilon \sim \dots \sim 100 \times W^{-6}$ is sufficient, as is often the case, counting times could be reduced by a factor $\times 6$ ($C_T \sim 700$, peak height ~ 100) and the number of measurement locations could be correspondingly increased.

Optimisation of peak parameters - To optimise counting times the required strain uncertainty should be specified. Peak parameters, such as counting time, step size and angular range, should then be chosen so as to enable the specified uncertainty value to be attained. Shorter counting times can be used if instrumental peak widths are low and detector angles are high.

12.2.3 Mapping

The number and spacing of points required adequately to define the required detail in a residual strain line scan depends upon whether the strain gradient is rapidly or gradually varying. The spacing problem is similar to that of other signal sampling and reconstituting situations so it is possible to use sampling theory to estimate an optimum step resolution [9].

the general form of the strain variation is known in advance step sizes may be chosen so that spatial resolution is appropriate. A common practical approach, if the form of the strain pattern is unknown, is to make a coarse step scan which is then fined by an appropriate function that interpolates between neighbouring points and to fill in with finer steps if it appears to be necessary. A similar approach is used when area mapping but with a function that interpolates in two dimensions, in this case, data of somewhat lower quality can be used as the interpolation will effectively be between four or more neighbouring points, rather than just two when line scanning. However, care should be taken with commercially available fining routines to ensure that the fitting algorithm is appropriate, in some cases routines fit exactly at experimental data points and generate spurious oscillations **in between**. The appropriateness of a fining routine can be judged by superimposing the locations of data points on the map and observing whether the map is overly distorted by the mapping matrix, if it is, another fitting routine or scanning matrix should be used.

12.2.3.1 Variable step mapping

In regions of low strain gradient variation the step size between points can be much greater than in regions of high strain gradient variation. However, if substantially varying step sizes are used, it can lead to apparent features on the strain map which are related to the variations in the mapping matrix rather than to the strain field. Distorting features appear as a result of the statistical uncertainties associated with any experimental measurement. If experimental points are close together, rapid uncertainty fluctuations will be observed on the map. If the points are well spaced out, the fining routine will interpolate a smooth variation between the distant points.

The visually distorting effect of uneven mapping is illustrated in Figures 12.1 and 12.2, Figure 12.1 shows two mapping matrices, one a regular square matrix and the other a more complex pattern in which the spacing varies by a factor of 10. Figure 12.2 shows the effects produced on a random number array pattern by using the two mapping matrices. Figure 12.2(a) is the full regular map with the expected randomly uneven pattern, figure 12.2(b) uses the same array of random numbers but is based on the partial irregular matrix obtained by omitting some of the points, 1/10 of the six small square regions fully mapped in both figures have been outlined to permit a direct visual comparison. Within the small squares both maps are essentially identical. In the intervening rectangular areas, similar to the one shown outlined, streaked patterns are generated as the periodicity in one rectangular direction is 10x that in the other. In the other areas of Figure 12.2(b), a variety of smoother larger scale patterns related to the more spaced mapping matrix, and random variations are evident.

When a strain map is generated from data collected at a matrix of points, the uncertainties in each data point will cause a spurious matrix-related pattern to be superimposed upon the 'true' strain map. If an area strain pattern is generated from an irregular matrix combination of coarse and fine steps between points, such as shown in Figure 12.1 (b), the effect can be particularly visually misleading, in general if a strain field contains distinct high and low strain gradient regions in which high and low density mapping is respectively appropriate, it is advisable to present the results on several maps rather than just one. For example, if the matrix in Figure 12.1(b) was used to collect the data, the results could be presented as six regular 10 x 10 small squares and one regular 10 x 10 large square. The former would give detailed pictures of each of the six small regions, the latter would only use a small proportion of the data collected but would give an undistorted low-resolution large-scale view.

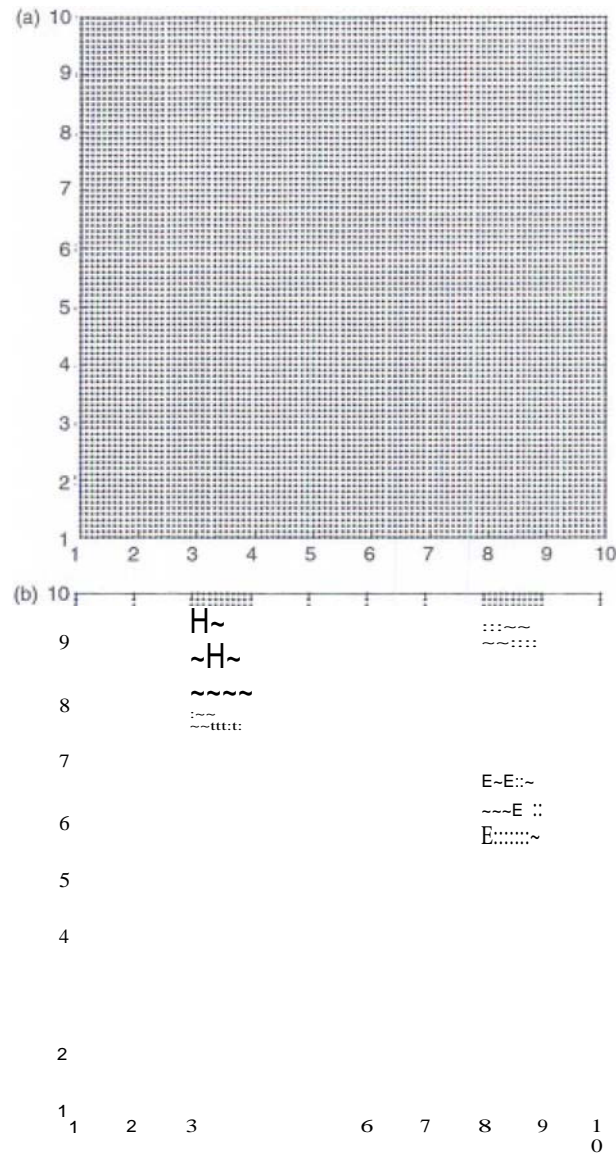


Figure 12.1 (a) Regular square matrix of 100 x 100 points. (b) Sparse matrix comprising small symbols and linear arrays of points of the 100 x 100 matrix shown in (a). (These matrices were used to generate the corresponding interpolated maps shown in Figure 12.2.)

12.3 Neutron diffraction

Figure 12.3 shows one of the first residual stress maps to be derived from two-dimensional neutron strain data. The data were collected using DIA at the ILL, Grenoble, in its single detector strain scanning mode [9]. Measurements were made over the head of a transverse railway rail section 12 mm thick using the 211 reflection in the three symmetry orientations,

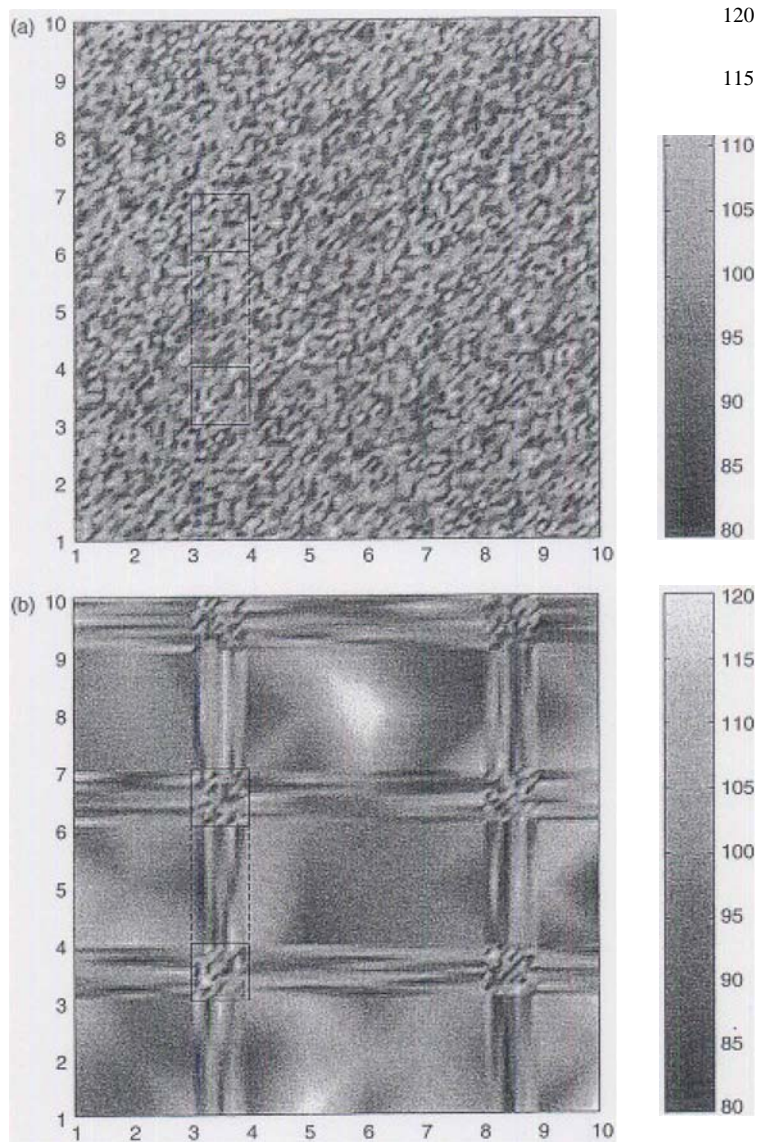


Figure 12.2 Interpolated 1024x1024 of 100 x 100 numbers, each 1024x1024 of value 100 but with a randomly generated Gaussian noise with a standard deviation 10: (a) arranged on the matrix shown in Figure 12.1 (a); (b) arranged on the matrix shown in Figure 12.1 (b) with the non-marked dam points omitted.

longitudinal, transverse and vertical using a near cubic sampling volume of side 2mm. The scans were made in nine parallel lines from $z = 0$ at the top of the bead to a depth of $z = 40$ mm at transverse locations $y = 0, \pm 8, \pm 16, \pm 24$ and ± 30 mm. Increments between points were varied from 2 mm near the top surface to 6 mm near $z = 40$ mm as strain gradients were known to be substantially higher near the top surface.

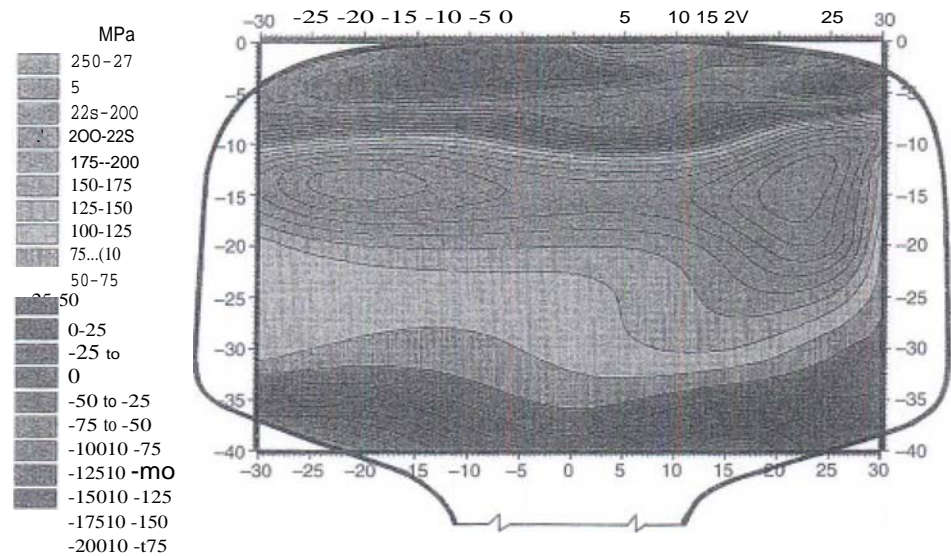


Figure 12.3 Transverse residual stresses in a BR rail head measured using D1A (ILL, Grenoble, Sec Colour Plate VI.)

The rail, which had been used, was taken from a straight section of British Rail (BR) track. The 'running line', the line of contact between wheel and rail, was centred at $y = +6$ mm. The map shows the computed interpolated transverse residual stress pattern which varies from +275 MPa in the central tensile band to -225 MPa in the compressive near-top surface region. The residual stress pattern is generally beneficial as the compressive outer layer inhibits the propagation of fatigue cracks from surface defects and the internal balancing tensile region does not reach the surface. The pattern shows some asymmetry due to the running line being 6 mm off-centre.

There is no apparent evidence of spurious features due to the scanning matrix. This is because the statistical data quality was relatively high and the uncertainties small, typically ± 25 MPa, the step sizes were almost constant in y , changed smoothly in z and were matched to the strain gradients. The first interpolation attempted showed distinct nodes at the line locations $y = 0, \pm 8, \pm 16, \pm 24$ and ± 30 mm and oscillations in between because it was constrained to fit exactly at the measured point and to change smoothly in between. The interpolation routine was subsequently revised so that fitting at the measurement points was allowed to vary within a standard deviation. The resulting smoother pattern may be considered to be a good representation as it shows no apparent evidence of features related to the measuring matrix but does reveal significant detail in the residual stress pattern.

12.4 Synchrotron X-ray strain mapping

Figure 12.4 shows results from a synchrotron X-ray study using the high-resolution diffractometer BM16 at the ESRF, Grenoble, with its single detector with analyser strain scanning mode [10]. The sample was a 10 mm thick transverse cross-section cut from a double-V multipass weld made in an aluminium alloy plate 4 mm thick. Scans were made in the transverse orientation using an incident beam 1 mm and a 1 mm high detector slit. The reflection used

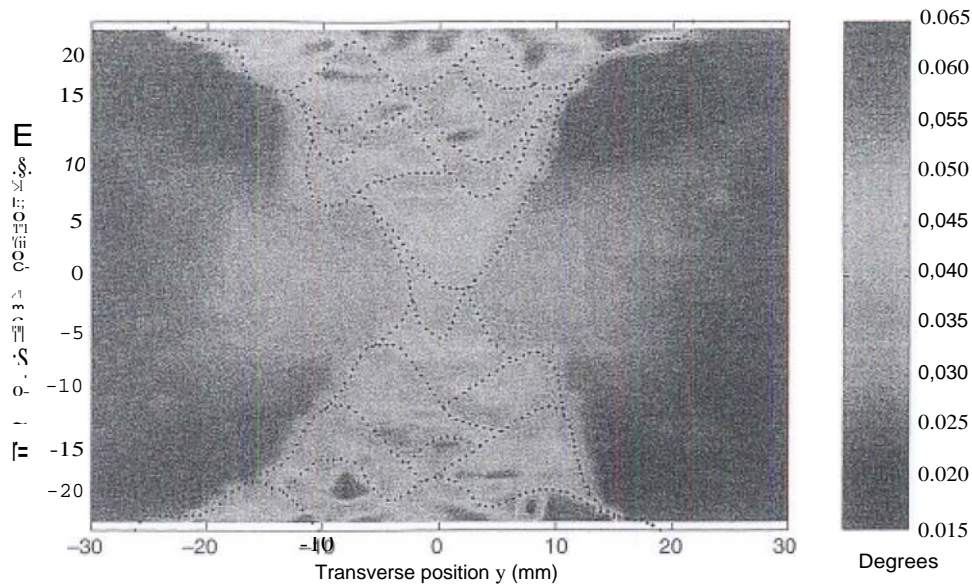


Figure 12.4 Peak width variation over a cross-section of an aluminium alloy double-V multipass weld measured using BM 16 at ESRF, Grenoble. The weld bead pattern is superimposed, (See Colour Plate VU.)

was 3 J], which at a wavelength 0.32, gave a gauge ~ 8 μm long in the longitudinal direction at a detector angle $\sim 15.1^\circ$. The measurements were made at mid-plane over a regular square matrix of points spaced at 1.333 mm intervals. In this particular case, as the longitudinal stresses had been substantially relaxed by the sectioning and were not expected to change significantly through the thickness, the elongated shape of the gauge was advantageous as it gave a better average, a higher count and less grain size variation. The 1 mm y and z gauge dimensions, and the matrix spacing, were chosen to be significantly smaller than the weld bead dimensions so that intra- and inter-bead, as well as fusion zone, boundary variations could be observed.

Figure 12.4 shows the multipass weld bead pattern superimposed upon the measured peak widths which are a measure of microstrain. The passes were made in layers alternately on top and bottom sides so that the weld was as symmetrical as possible. The central layers are thus partially annealed by subsequent passes but the surface passes are not. The bead pattern was not entirely regular and the fusion zone boundaries were neither straight nor symmetrical. The step size was sufficiently small, and the gauge was so well defined, that the map reveals several significant features. There is a clear correlation between the peak widths and details of the weld such as the edge of the fusion zone and the individual weld beads. At transverse distances $y > \sim 0$ mm from the weld the peaks are uniformly ~ 0.015 wide, which corresponds to the inherent instrumental resolution and low microstresses in the plate prior to welding. The increases in peak widths elsewhere are mainly a measure of microstrains and, to a small extent, macrostrain gradients resulting from the welding process and plastic deformation. The maximum peak broadening, 0.065, corresponds to a microstrain of $\sim 3 \times 10^{-3}$. The fusion zone boundary is outlined in detail by a narrow layer, about one matrix step wide, in

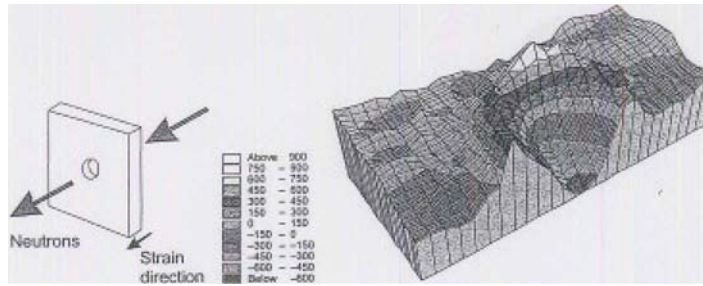
which peak widths are $\sim 0.04^\circ$. This indicates that the microstrain change at the boundary is generally very sharp and is less than or equal to the spatial resolution. Outside the weld roughly within the band $-20 < Y < 20 \text{ mm}$, $-5 < Z < 5 \text{ mm}$, there is another region in which peak widths are similarly $\sim 0.04^\circ$. In this region there has probably been some plastic deformation as it would have been initially in tension as the first beads were laid down, but finally became a balancing compressive region as later beads were laid. Inside the weld, peak widths vary from $\sim 0.04^\circ$ in the partially annealed near mid-thickness region to $\sim 0.065^\circ$ in the last deposited surface beads where microstrains are highest.

12.5 Conclusions

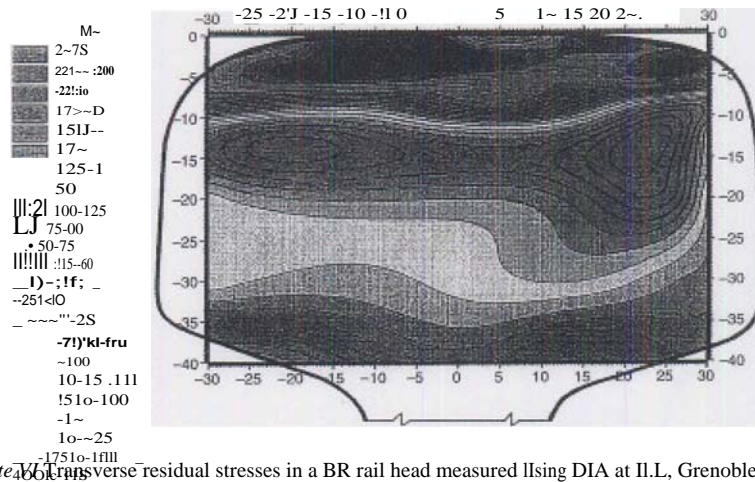
Two-dimensional strain mapping is becoming increasingly common using both neutrons and synchrotron X-radiation. This development is a result of demand from engineers, who are now beginning to insist on detailed residual strain and stress information so as to be able to refine their designs and to validate their modelling codes and the increasing ability of strain scanners now to supply large amounts of repeatable data at acceptably low unit cost. It is anticipated that demands will continue substantially to increase and that standardisation and scanner design, measurement techniques, automated data processing and analysis will develop so that non-destructive residual strain and stress mapping of components will become as routine and essential in engineering as body scanning is now in medicine.

Reference

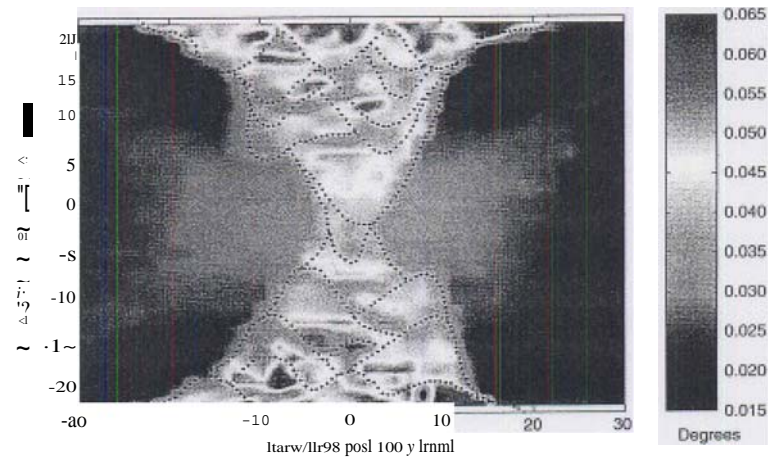
- [1] Allen A., Andreani C., Hutchings I. T. and Windsor C. G. Measurement of internal stress within bulk materials using neutron diffraction. *NDT Int.* 14, 249-254 (1981).
- [2] Plutschovius L., Jung V., Macherand E. and Vohlinger O. Residual stress measurements by means of neutron diffraction, *Mater. Sci. Eng.*, 61, 43-50 (1983).
- [3] Tracey A., MacChlery H. L., Webster G. A., Webster P. J. and Ziebeck K. R. A. Measurement of residual stresses by neutron diffraction, *J. Strain Anal.*, 20, 93-100 (1985).
- [4] Webster P. J., Mills G. and Wang X. D. Residual strain scanning of engineering samples. *SRS Annual Report 1121/40 A65* (1992/93).
- [5] Webster P. J. Strain scanning using X-rays and neutrons, *Mater. Sci. Forum*, 228-231, 191-200 (1996).
- [6] Webster P. J. Neutron strain scanning, *Neutron News*, 2, 19-22 (1991).
- [7] Webster P. J., Mills G., Wang X. D., Kang W. P. and Holden M. Neutron strain scanning of a small welded austenitic stainless steel plate, *J. Strain Anal.*, 30, 35-43 (1995).
- [8] Webster P. J. and Kang W. P. Optimisation of neutron and synchrotron data collection and processing for efficient Gaussian peak fitting. *Engineering Science Group Technical Report ESG/98*, The Telford Institute of Structures and Materials Engineering, University of Salford, March 1998.
- [9] Kang W. P. Application of numerical analysis to neutron strain scanning, PhD Thesis University of Salford, August 1996.
- [10] Webster P. J., Vaughan G. B. M., Mills G. and Kang W. P. High-resolution synchrotron strain scanning at BM16 at the ESRF, *Mater. Sci. Forum*, 218-281, 323-328 (1998).



Colour Plate V Map of the strain field around a 6 mm diameter cold-expanded hole in a ferritic steel, measured by the Bragg-diffraction transmission technique at ISIS, UK. (See Figure 11.15, page 204.)



Colour Plate VI Transverse residual stresses in a BR rail head measured using DIA at ILL, Grenoble. (See Figure 12.3, page 216.)



Colour Plate VII Peak width variation over a cross-section of an aluminium alloy double-V multipass weld measured using BM 16 at FSRF, Grenoble. The weld bead pattern is superimposed. (See Figure 12.4, page 217.)